

# An algorithm for obtaining the frequency and the times of respiratory phases from nasal and oral acoustic signals

Guillermo Kemper, Angel Oshita, Ricardo Parra, Carlos Herrera

School of Electronic Engineering, Faculty of Engineering, Universidad Peruana de Ciencias Aplicadas, Lima, Peru

## Article Info

### Article history:

Received Mar 4, 2022

Revised Jul 19, 2022

Accepted Aug 15, 2022

### Keywords:

Breathing rate

Buccal sound

Envelope detection

Expiration time

Inspiration time

Nasal sound

Respiration

## ABSTRACT

This work proposes a computational algorithm which extracts the frequency, timings and signal segments corresponding to respiratory phases, through buccal and nasal acoustic signal processing. The proposal offers a computational solution for medical applications which require on-site or remote patient monitoring and evaluation of pulmonary pathologies, such as coronavirus disease 2019 (COVID-19). The state of the art presents a few respiratory evaluation proposals through buccal and nasal acoustic signals. Most proposals focus on respiratory signals acquired by a medical professional, using stethoscopes and electrodes located on the thorax. In this case the signal acquisition process is carried out through the use of a low cost and easy to use mask, which is equipped with strategically positioned and connected electret microphones, to maximize the proposed algorithm's performance. The algorithm employs signal processing techniques such as signal envelope detection, decimation, fast Fourier transform (FFT) and detection of peaks and time intervals via estimation of local maxima and minima in a signal's envelope. For the validation process a database of 32 signals of different respiratory modes and frequencies was used. Results show a maximum average error of 2.23% for breathing rate, 2.81% for expiration time and 3.47% for inspiration time.

This is an open access article under the [CC BY-SA](https://creativecommons.org/licenses/by-sa/4.0/) license.



## Corresponding Author:

Guillermo Kemper

School of Electronic Engineering, Faculty of Engineering, Universidad Peruana de Ciencias Aplicadas

Lima 15023, Peru

Email: guillermo.kemper@upc.pe

## 1. INTRODUCTION

Most diseases related to an obstructed or restricted respiratory system can be characterized by the sounds generated during breathing. These include asthma, chronic obstructive pulmonary disease (COPD), among others [1]. Airway abnormalities can cause abnormal breathing sounds. Examples of this could be the absence of unusual or additive sounds, which are known as continuous adventitious sounds (CAS) [2]. Moreover, most analysis procedures for these ailments require auscultation and depend on the skill and experience of the medical professional [3]. Therefore, there has been a significant effort to research the acoustics of respiration and develop techniques that aid in the diagnosis of respiratory ailments. An expert on auscultation needs to have lot of experience in order to be able to classify the types of sounds and decide on how this information can help in diagnosis or monitoring [4]. Symptoms might be missed, and their severity underestimated by both patients and physicians [5], resulting in proper care not being given. Besides, many evaluation procedures are done on-site with a stethoscope. Other devices such as spirometers can measure respiratory flow and rate, and thorax monitoring equipment with sensors and electrodes can analyze sound signals and waveforms to detect a possible pathology. Nonetheless, these evaluations need to be done on-site

and with the aid of a medical professional, because it is complicated for a patient to have the required equipment as well as to be able to accurately acquire the signals.

In this context, the proposed algorithm aims to be part of a simple and low-cost product that can evaluate a patient either remotely or on-site, regarding the breathing rate and the timings of respiratory phases. This will enable the estimation of aspired/expired air volume in each respiratory phase, the segmentation of waveforms and the analysis of possible pathologies. Thus, this work develops a computational solution for medical applications which require the monitoring, evaluation and on-site or remote tracking of patients with pulmonary ailments such as coronavirus disease 2019 (COVID-19). The objective is to build an easy-to-use application for mobile, desktop, web server or small single-board computer-based systems. It is important to note that, in order to maximize the algorithm's performance, the acoustic signals must be acquired via the low-cost mask equipped with strategically located and connected microphones, which is also described in this work.

The scientific literature presents proposals that aim to solve the described problem. For example, Nam *et al.* [6] proposed a method which detects air flow with a microphone located below the nose, to estimate the breathing rate by averaging the power of the nasal respiratory signals in each phase. The method uses two spectral analysis techniques on the sound envelope: the Welch periodogram and the autoregressive spectrum. Results show the method is highly precise for the considered breathing rate range (6-90 respirations/min), with a low average error of less than 1%. Nonetheless, the method struggles to detect low frequency components.

Li *et al.* [7] proposed an algorithm to estimate frequency parameters and characteristics for wheezing detection. It uses the Fisher's linear discriminant analysis algorithm to separate wheezing sounds from regular respiratory sounds, resulting in a sensibility and positive predictive rate of 91.51% and 100% respectively. The algorithm only uses short-term data or a few respiratory sound samples, so the computational complexity is low.

On the other hand, Yahya and Faezipour [8] used a support vector machine (SVM) to automatically detect and distinguish between inspiration and expiration phases without air flow measurements. The respiratory signal is processed via the voiced-dull algorithm to distinguish between a voiced period or a dull period (silence). The features of interest are extracted from each voiced phase and are used to train the SVM, achieving a classification precision of 95%. Nonetheless, this algorithm only works for deep respirations.

Nam *et al.* [9] presented an algorithm to estimate the resting breathing rate directly from light intensity fluctuations from a pulsed light source captured by a smartphone camera, achieving a precision of 95%. However, precision falls when respiration rate exceeds 30 respirations/min. Meanwhile, Chatterjee *et al.* [10] develop an algorithm to detect respiratory phases from audio data. They transform the signals into spectral-temporal images and train a wheezing detection model based on convolutional neural networks (CNN), achieving a precision of 96.99%, specificity of 97.96% and a sensibility of 96.08%. Nonetheless, the training dataset is limited which restricts the model to only 2 convolutional layers.

Avalur [11] presented a respiration detection and analysis algorithm which classifies a person's respiration into soft, light, and hard, and estimates the breathing rate with a precision of 94.68%. The main limitations are a high sensitivity to background noise and a reduced performance with high amplitude errors. Furthermore, algorithms for feature extraction and analysis of breath sounds in the temporal, spectral and time-frequency domains are proposed in [12], [13]. Nonetheless, Díaz *et al.* [12] did not report any sensibility or precision results and in study [13], the algorithm detects respiration peaks with a precision of 94.5%.

Javed *et al.* [14] presented ResCSRF, which takes 4 signals (nasal flow, thorax, abdomen, and finger oxygen saturation) as input. It first detects corporate social responsibility (CSR) cycles and then calculates the respiratory features (cycle-length, lung-to-periphery circulation time. and time to peak flow). It outputs nightly statistics (mean, median, standard deviation, and percentiles) of these features. It was developed and blindly tested on a group of 49 chronic heart failure patients undergoing overnight in-home unattended respiratory polygraphy recordings].

Islam and Lubecke [15] investigated the feasibility of using the independent components analysis-joint approximation diagonalization of eigen-matrices (ICA-JADE) algorithm with a 24 GHz phase comparison monopulse radar transceiver for separating respiratory signatures from combined mixtures of varied breathing patterns. Meanwhile, Sun *et al.* [16] proposed an adaptive boosting (AdaBoost) method based on the multi-layer neural network (MLP-NN) to predict the respiratory signal accuracy in our previous study. The experiment results demonstrated that the appropriate AdaBoost method based on MLP-NN could predict the respiratory signal accuracy.

The proposed algorithm in [17] is based on the analysis of the respiratory rate variability (RRV) to detect difficulties in falling asleep. Moreover, a method to provide a quality level of the respiratory signal is also proposed. Both methods have been combined to reduce false alarms due to the changes of measured RRV associated not with drowsiness but body movements.

The proposed method in [18] has adopted several vital parameters to quantify respiratory patterns and updated all the baselines dynamically while Saatci and Saatci [19] used Hurst exponent to reveal the fractal properties of respiratory signals and respiratory sound signals and to estimate the pressures in the respiratory system. The combination of well-known statistical signal processing methods and optimization were applied to the experimentally acquired 23 records. Oletic and Bilas [20] proposed quantification of wheezing by a sensor system consisting of a wearable wireless acoustic sensor and smartphone performing respiratory sound classification, may contribute to the diagnosis, long-term control, and lowering treatment costs of asthma.

On the other hand, the aim of Paraschiv and Rotaru's research [21] was to present some related works that have been made in this field and the proposed method for classifying the International Conference on Biomedical and Health Informatics 2017 (ICBHI'17) scientific challenge respiratory sound database. The method included the extraction of features using Mel-frequency cepstral coefficients (MFCC) and computing a CNN to classify the database. The results reveal that the proposed method serves an accuracy of 90.21% which provides a suitable method to faster classify any respiratory sounds collected from different devices.

Wang *et al.* [22] may contribute to the development of low-cost and non-contact respiratory monitoring products specific to home or work health care. To achieve low-cost and remote measurement of respiratory signal, a red-green-blue (RGB) camera collaborated with marker tracking is used as data acquisition sensor, and a Raspberry Pi is used as data processing platform. To overcome challenges in actual applications, the signal processing algorithms are designed for removing sudden body movements and smoothing the raw signal.

Bokov *et al.* [23] used an SVM classifier to perform wheezing detection. The signals were obtained with a single microphone (SP0410HR5H-PB) which recorded mouth breath sounds. A total of 95 recordings were collected, with 27 of them containing wheezes. 70 recordings with wheezes in 20 of them, were used to train the SVM classifier while the rest were used to test the classifier. Spectral-based features were used for the classifier. The recordings were divided into segments and the features were extracted from each frame of the segmented recordings. Using this method, 71.4% sensitivity and 88.9% specificity were achieved on the validation set at the recording level.

Finally, Sierra *et al.* [24] developed a non-invasive method for continuously monitoring respiratory rate (RR) based on tracheal sounds. Tracheal sounds were acquired using a contact piezoelectric sensor placed on the examinee's throat and analyzed using a combined investigation of the sound envelope and frequency content. RR estimates were compared to reference measurements taken from a pneumotachometer coupled to a face mask worn by the examinee. RR was also manually counted by a respiratory technician. Two types of breathing (mouth and nose) and three different positions were studied. RR estimated in volunteers had a success rate of 96%, a correlation coefficient of 0.99 and a standard error of the estimate of 0.56.

As can be seen, there are different proposals that aim to detect characteristics and pathologies from the mouth or nasal sound of breathing, applying in most cases signal processing techniques and artificial intelligence. Moreover, different algorithms work in portable devices such as smartphones or tablets due to their low complexity. The results obtained in the scientific literature have been satisfactory although in some cases they were only evaluated with signals available in databases. Also, many algorithms have limitations due to noise and distortion generated in the signal acquisition process.

In this context, the main contribution of the proposed work is focused on the signal acquisition method (buccal or nasal), with the objective of improving the breathing rate and timing interval estimation precision. Moreover, the acquisition method employs a KN95 mask and electret microphones, which are a low-cost solution for patients to acquire the signals by themselves via a microphone, personal computer, or portable device without the aid of medical professionals. Another contribution is that the proposed algorithm has a very low complexity level and can be easily ported to mobile and portable devices without the need of high-performance processors or expensive memory requirements. The algorithm's validation was developed with 32 signals corresponding to 3 different people. The average maximum relative error for different breathing rates and periods was 2.23%, while the same metric for expiration and inspiration timing intervals was 2.81% and 3.47% respectively. Results are satisfactory and show a good performance of the proposed method. The following sections describe the parts and stages that are part of the method, as well as report on the results and conclusions.

## 2. PROPOSED METHOD

Figure 1 shows the block diagram of the proposed algorithmic method. The first two blocks (signal acquisition and signal segmentation) are explained jointly in section 2.1. The rest of the blocks are each explained separately in sections 2.2. through 2.5.

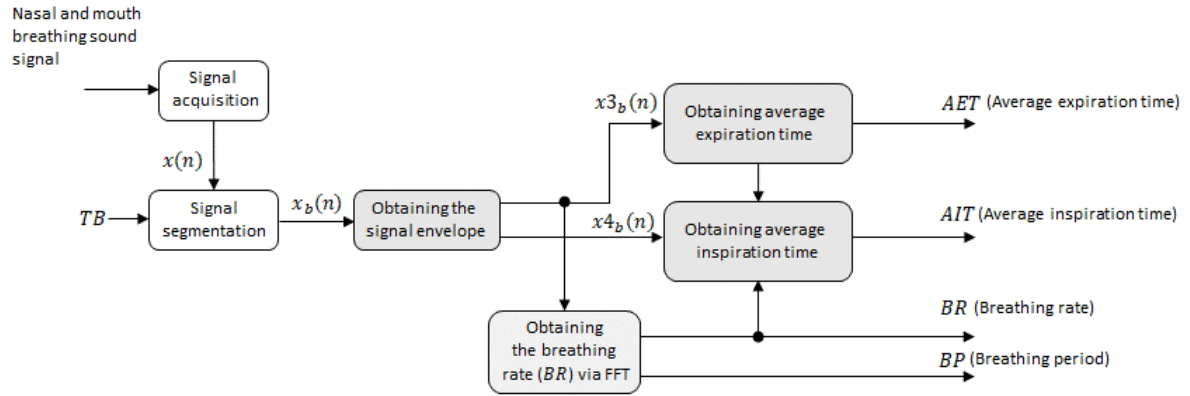


Figure 1. Block diagram of the proposed algorithm

**2.1. Signal acquisition and segmentation**

As previously stated, the respiration acoustic signal is acquired via electret microphones installed on a KN95 mask, as shown in Figure 2. Figure 2(a) shows a drawing of a person using the mask. Figures 2(b) and 2(c) show the acquisition device in nasal configuration and buccal configuration respectively. Finally, Figure 2(d) shows the schematic diagram of the microphone electrical circuit. Note that each microphone stands on a small structure designed to support it, which allows adequately fixing them on the KN95 mask. The microphone placement is crucial, because it enables acquiring an adequate acoustic signal to extract the breathing rate and the inspiration and expiration timings.

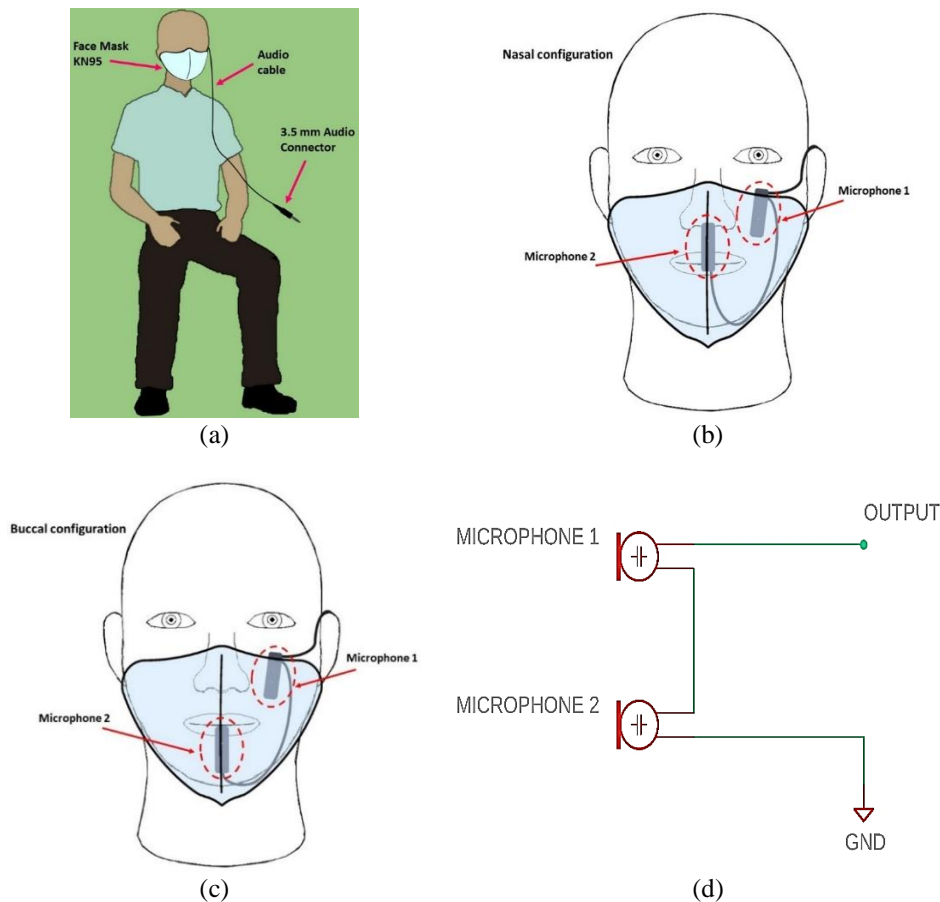


Figure 2. Signal acquisition mask (a) placed on a person, (b) nasal microphone configuration, (c) buccal microphone configuration, and (d) microphone electrical circuit

Microphone placement must satisfy the following requirements: microphone 1 must always be located to one of the sides of the mask as shown in Figures 2(a) and 2(b), while microphone 2 must be located facing one of the orifices through which the person will expire (nasal or buccal configuration). Figure 2(d) shows the electrical circuit diagram of the microphones, which are then connected to the input of an audio card. In this case, a personal computer card can be used, as well as that of a mobile phone or an audio USB adapter for a reduced board computer. The digitization parameters were a sampling frequency of  $f_s=8000$  Hz, 16 bits per sample and mono audio channel. The use of the lowest possible sampling frequency available in audio cards is justified because the maximum normal breathing rate must be close to 25 cycles/minute (0.41 Hz) while it must be close to 60 cycles/minute (1 Hz) for a baby [25].

Figure 3 shows an example of an acoustic respiration signal  $x(n)$  acquired through the microphone array device. The expiration signal will always have a larger amplitude than the inspiration signal due to microphone 2, which is an important attribute to distinguish between each respiratory phase. Figures 4 and 5 show signals acquired with an open mask (as if no mask were present).

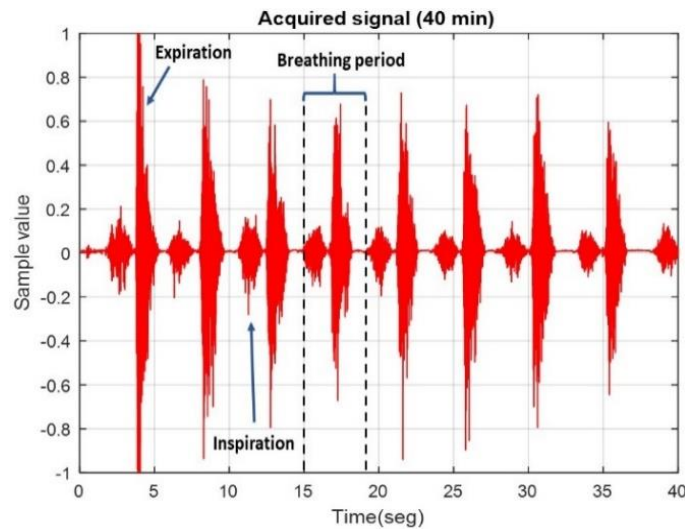


Figure 3. Acquired signal of breathing sound (with mask)

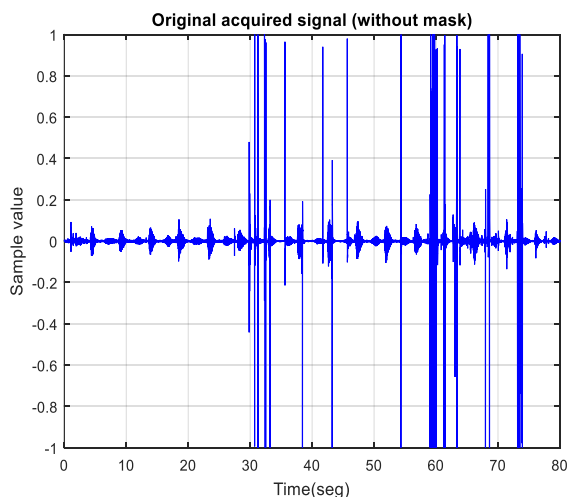


Figure 4. Acquired signal of breathing sound (without mask)

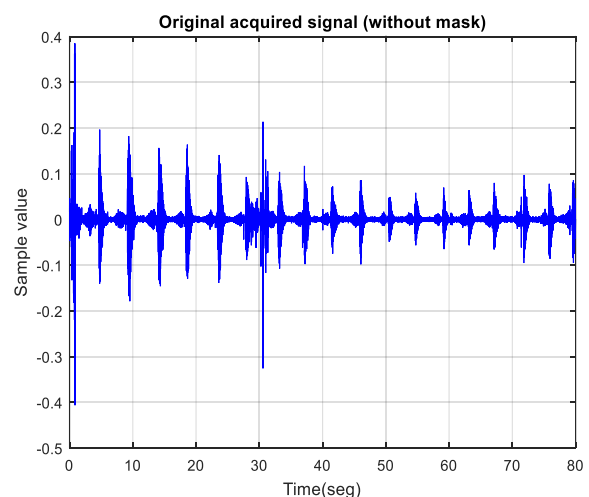


Figure 5. Acquired signal of breathing sound (without mask)

Note that signals acquired are much more affected by noise in the acquisition environment. Noise usually generates distortion in the signal envelope due to the presence of overpulses. Also, when added to the

acquired respiration signal, it makes it difficult to differentiate the inspiration and expiration phases [26]. All this ends up significantly affecting the performance of the proposed method (based on envelope detection), so it is essential to use the acquisition mask, in order to maximize the signal-to-noise ratio (SNR) of the acquired signal and obtain results and measurements with a very low percentage of error. The mask equipped with the electret microphones, microphone support structures, audio cables and the 3.5 mm audio jack have an estimated price of US\$5.00, which is an affordable price for a patient, considering that the device is of strictly personal use due to health reasons.

## 2.2. Obtaining the signal envelope

Figure 3 shows that the inspiration and expiration periods and timings are easily detectable from the signal envelope. Starting from this observation, two signal envelopes were extracted. The first one highlights the expiration timings and the signal periodicity. The second one highlights the same parameters but for the inspiration signal. This last step is important to reduce the error in timing detection of inspiration phase signals.

The envelope extraction procedure is explained in the following sections: Step 1, the input signal  $x(n)$  is processed block-by-block with a block duration of  $TB = 40$  seconds, which translates into a total of samples per block of  $NSB = f_s \times Tb = 8,000 \times 40 = 320,000$ . Although the block time duration can be configured, a minimum of 40 seconds is recommended because an appropriate detection of respiratory parameters requires an adequate quantity of signal periods. A signal block  $x_b(n)$  corresponding to block  $b$  can be expressed as (1) [27].

$$x_b(n) = x(n + b.NSB), \text{ for } n = 0,1,2, \dots, NSB - 1, \quad b = 0,1,2, \dots, NB - 1 \quad (1)$$

Where  $NB$  is the number of blocks in the acquired signal.

Step 2, a linear phase finite impulse response (FIR) filter with impulse response  $h1(n)$  is used to filter signal block  $x_b(n)$  to obtain its envelope and decimate the sampling frequency by a factor of  $M = 200$ . This required a cutoff frequency of  $\theta1_c = \pi/M$  and a very high filter order of 4000 due to the narrowband nature of the signal. Decimation enabled the decrease of the number of samples to process and reduced the fundamental Nyquist range to  $[-20 \text{ Hz}, 20 \text{ Hz}]$ , which is enough for the low frequency respiratory signals. The decimated envelope signal  $x2_b(n)$  can be expressed as (2) [27].

$$x2_b(n) = x1_b(Mn), \text{ for } n = 0,1, \dots, NSBB - 1 \quad (2)$$

Where  $x1_b(n)$  results from the convolution:

$$x1_b(n) = |x_b(n)| * h1(n) \quad (3)$$

$$NSBB = \frac{NSB}{M} \quad (4)$$

In this case, if  $NSB = 320,000$ , then  $NSBB = 1,600$ . The sampling frequency after decimation is  $f_{s1} = \frac{f_s}{M} = \frac{8000}{200} = 40 \text{ Hz}$ . Sometimes, undesired high frequency undulations may compromise the interval detection for expiration signals. In these cases, signal  $x2_b(n)$  was filtered by a low-pass filter with impulse response  $h2(n)$ , order 4,000 and cut-off frequency of  $\theta2_c = \pi/10$ . The resulting signal can be expressed by (5).

$$x3_b(n) = x2_b(n) * h2(n) \quad (5)$$

Figure 6 shows  $x3_b(n)$  for the signal in Figure 3. Figure 6 also shows that the expiration intervals are evident in  $x3_b(n)$ , which will later help in detecting them. The inspiration phase signals may present a high attenuation, which hampers their detection in  $x3_b(n)$ . Thus, a fourth signal envelope was computed using a FIR filter with impulse response  $h3(n)$ , order 4,000 and a cut-off frequency of  $\theta3_c = 2\pi/5$ . This larger bandwidth resulted in a filtered envelope with a larger amplitude and detail for the inspiration phase. The signal can be expressed as (6).

$$x4_b(n) = x2_b(n) * h3(n) \quad (6)$$

Figure 7 shows  $x4_b(n)$  for the signal in Figure 3. Note the larger y-axis with respect to Figure 6, such that the inspiration phase has a larger amplitude and detail.

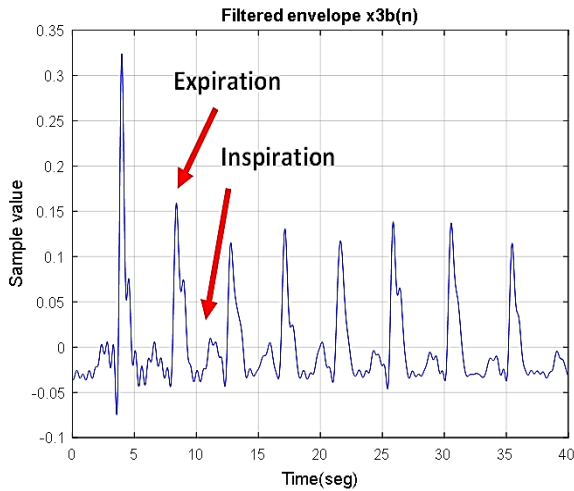


Figure 6. Filtered envelope  $x3_b(n)$  obtained from the signal shown in Figure 3

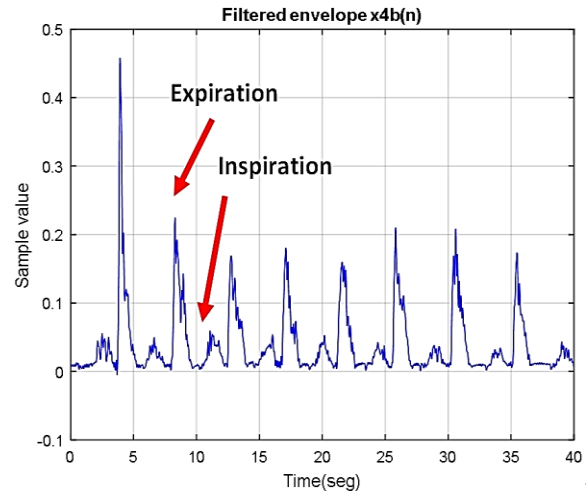


Figure 7. Filtered envelope  $x4_b(n)$  obtained from the signal shown in Figure 3

### 2.3. Obtaining the breathing rate via FFT

The breathing rate was computed through the discrete Fourier transform (DFT) of envelope  $x3_b(n)$  because it shows the breathing rate more clearly through the expiration phases. Firstly, the DC component of the signal was eliminated, since the detection consists of finding the largest frequency component at a frequency different than zero. A Hamming window was used to reduce the block effects, since the transform is applied to the envelope of each signal block. The transformation was computed by the fast Fourier transform (FFT). The modulus of the frequency spectrum in the Nyquist interval can be expressed as (7) [28].

$$AX3_b(k) = \left| \sum_{n=0}^{NSBB-1} xv3_b(n) \cdot e^{-j\frac{2\pi kn}{N}} \right|$$

$$k = 0, 1, 2, \dots, \frac{N}{2} - 1 \quad (7)$$

Where

$$xv3_b(n) = (x3_b(n) - mx3_b) \cdot w(n) \quad (8)$$

$$mx3_b = \frac{1}{NSBB} \sum_{n=0}^{NSBB-1} x3_b(n) \quad (9)$$

$$w(n) = 0.54 - 0.46 \cos\left(\frac{2\pi n}{NSBB-1}\right)$$

for  $n = 0, 1, 2, \dots, NSBB - 1$  (10)

In this case, due to  $NSBB = 1,600$ , a transform size of  $N = 2,048$  was used so that it could be computed via FFT ( $N$  being a power of 2). The  $k_0$  position corresponds to the largest frequency component and must fulfill the following condition:

$$AX3_b(k_0) > AX3_b(k), \quad \forall k \neq k_0 \quad (11)$$

The computation of the breathing rate  $f0_b$  (Hz) for block  $b$  can be expressed as:

$$f0_b = k_0 \times \frac{fs1}{N} \quad (12)$$

And the breathing period  $T0_b$  in seconds will be:

$$T0_b = \frac{1}{f0_b} \quad (13)$$

For every acquired signal, the average breathing period (in seconds) is expressed by (14).

$$BP = \frac{1}{NB} \sum_{b=0}^{NB-1} T0_b \quad (14)$$

Figure 8 shows the spectrum  $AX3_b(k)$  in Hz, for the signal envelope  $x3_b(n)$  in Figure 6. Finally, the breathing rate  $BBR_b$  for block  $b$  in cycles per minute is (15).

$$BBR_b = f0_b \times 60 \text{ cycles/minute} \quad (15)$$

For a complete acquired signal, the average breathing rate will be:

$$BR = \frac{1}{NB} \sum_{b=0}^{NB-1} BBR_b \text{ cycles/minute} \quad (16)$$

A look-up is done in the spectrum, starting from position  $k0_b$  and looking up to  $k = 6$  samples (corresponding to about 6 cycles per minute) in search of an amplitude higher than  $0.6AX3_b(k0_b)$ . If such an amplitude is found,  $k0$  is updated with the location of this new peak. This is done because, sometimes, the inspiration signal is larger than the expiration signal, which causes the 2<sup>nd</sup> spectrum harmonic component to be greater than the fundamental frequency component, which correctly defines the breathing rate.

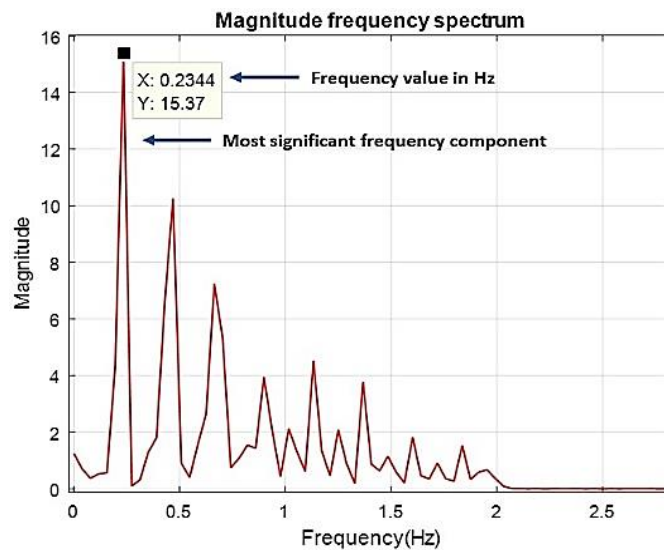


Figure 8. Magnitude frequency spectrum from  $xv3_b(n)$ , which was obtained from envelope shown in Figure 4

#### 2.4. Obtaining average expiration time

Envelope  $x3_b(n)$  is used to identify and segment the expiration interval. This envelope clearly shows the signal peaks thanks to the microphone distribution during signal acquisition. The algorithmic detection steps are explained.

Step 1: The number of expiration peaks  $NPE$  in a signal block is estimated through the block time duration  $TB$  and the calculated breathing rate  $f0$ :

$$NPE = \text{floor}(TB \cdot f0_b) \quad (17)$$

where  $\text{floor}(a)$  returns the lowest integer value closest to  $a$ .

Step 2: A counter is started in  $i = 0$  and a new discrete signal is generated,  $x33_b(n) = x3_b(n)$ .

Step 3: The position of the minimum value of  $x3_b(n)$  is obtained,  $nemin$ .

Step 4: The position of the minimum value of  $x33_b(n)$  is obtained,  $nemax$ .



Step 5: Position  $nemin1$  is obtained, corresponding to the minimum value of  $x3_b(n)$  between  $n = nemax + 1$  and  $n = NSBB - 1$ .

Step 6: Position  $nemin2$  is obtained, corresponding to the minimum value of  $x3_b(n)$  between  $n = 0$  and  $n = nemax - 1$ .

Step 7: A minimum decision threshold,  $temin1$ , is computed as (18):

$$temin1 = x3_b(nemin1) + 2demin1 \quad (18)$$

where:

$$demin1 = \frac{x3_b(nemax) - x3_b(nemin1)}{10} \quad (19)$$

Step 8: A minimum decision threshold,  $temin2$ , is computed as (20):

$$temin2 = x3_b(nemin2) + 2demin2 \quad (20)$$

where:

$$demin2 = \frac{x3_b(nemax) - x3_b(nemin2)}{10} \quad (21)$$

Step 9: The values of  $x3_b(n)$  are looked-up towards the right (increasing  $n$ ), from  $n = nemax$  until finding the first position where  $x3_b(n) < temin1$ . This position will be expressed as  $p2_b(i)$ .

Step 10: The values of  $x3_b(n)$  are looked-up towards the left (decreasing  $n$ ), from  $n = nemax$  until finding the first position where  $x3_b(n) < temin2$ . This position will be expressed as  $p1_b(i)$ .

Step 11:  $x33_b(n) = 0.5x3_b(nemin)$  for  $p1_b(i) \leq n \leq p2_b(i)$ .

Step 12: If  $i \leq NPE$  then  $i = i + 1$  and the procedure is repeated from step 4. Else, the procedure continues to step 13.

Step 13:  $p1_b$  y  $p2_b$  are sorted from smallest to largest. Figure 9 shows  $x3_b(n)$  with labels in the positions specified by  $p1_b$  and  $p2_b$ . A red label means the beginning of a respiratory phase and a blue label means its end.

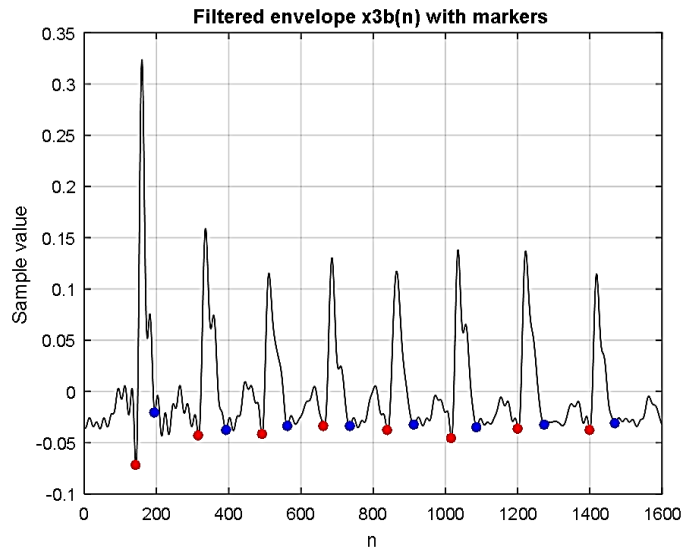


Figure 9. Filtered envelope  $x3_b(n)$  with markers at each expiration interval: red (start) and blue (end)

Step 14: The average expiration time  $AAET_b$  for block  $b$  is computed as (22).

$$AAET_b = \frac{1}{NPE} \sum_{i=0}^{NPE-1} \frac{(p2_b(i) - p1_b(i))}{fs1} \quad (22)$$

Finally, the average expiration time for the whole acquired signal is:

$$AET = \frac{1}{NB} \sum_{b=0}^{NB-1} AAET_b \quad (23)$$

## 2.5. Obtaining average inspiration time

Signal  $x_{4_b}(n)$  is used to identify and segment each inspiration interval, using position  $p_{1_b}(i)$  as the starting sample and position  $p_{2_b}(i)$  as the end sample for each expiration phase detected in the previous procedure. As previously stated, envelope  $x_{4_b}(n)$  has more detail in comparison to  $x_{3_b}(n)$ , which contributes to adequately detecting each inspiration interval. The procedure is described in the following section.

Step 1: Start a counter  $i = 0$ .

Step 2: The position of the maximum value in  $x_{4_b}(n)$  located between  $p_{2_b}(i)$  and  $p_{2_b}(i+1)$  is stored in position  $nimax$ . Then, the position of the minimum value in  $x_{4_b}(n)$  located between  $nimax$  and  $p_{2_b}(i+1)$  is stored in position  $nimin1$ . Finally, the position of the minimum value in  $x_{4_b}(n)$  located between  $p_{2_b}(i)$  and  $nimax$  is stored in position  $nimin2$ .

Step 3: A minimum decision threshold  $timin1$  is computed for the sample interval between  $nimax$  and  $p_{1_b}(i+1)$ :

$$timin1 = x_{4_b}(nimin1) + 2dimin1 \quad (24)$$

where

$$dimin1 = \frac{x_{4_b}(nimax) - x_{4_b}(nimin1)}{15} \quad (25)$$

Step 4: A minimum decision threshold  $timin2$  is computed for the sample interval between  $p_{2_b}(i)$  and  $nimax$ :

$$timin2 = x_{4_b}(nimin2) + 2dimin2 \quad (26)$$

where

$$dimin2 = \frac{x_{4_b}(nimax) - x_{4_b}(nimin2)}{15} \quad (27)$$

Step 5: A look-up is performed in envelope  $x_{4_b}(n)$ , starting from  $n = nimax$  towards the right until finding the first position where  $x_{4_b}(n) < timin1$ . This position is stored in  $p_{4_b}(i)$ .

Step 6: A look-up is performed in envelope  $x_{4_b}(n)$ , starting from  $n = nimax$  towards the left until finding the first position where  $x_{4_b}(n) < timin2$ . This position is stored in  $p_{3_b}(i)$ .

Step 7: If  $i \leq NPE - 1$ , then  $i = i + 1$  and the procedure repeats from step 2. Else, the procedure continues towards step 8. Figure 10 shows  $x_{4_b}(n)$  with red markers at the start and blue markers at the end of the detected expiration intervals. Moreover, there are yellow markers for the start and cyan markers for the end of the detected inspiration phases. A valid inspiration phase consists of a detected inspiration phase located between two consecutive valid expiration phases. Thus, there will always be one detected inspiration phase less than the number of detected expiration phases ( $i = 0, 1, \dots, NPE - 2$ ).

Step 8: The estimation of the average inspiration time  $AAIT_b$  for block  $b$  is then:

$$AAIT_b = \frac{1}{NPE-1} \sum_{i=0}^{NPE-2} \frac{(p_{4_b}(i) - p_{3_b}(i))}{fs1} \quad (28)$$

Finally, the average inspiration time for the complete signal can be expressed as (29).

$$AIT = \frac{1}{NB} \sum_{b=0}^{NB-1} AAIT_b \quad (29)$$

As previously mentioned, the aspired and expired air volumes can be estimated from the expiration and inspiration times. Positions  $p_{1_b}(i)$ ,  $p_{2_b}(i)$ ,  $p_{3_b}(i)$  and  $p_{4_b}(i)$  serve as timestamps to obtain interval masks on signal block  $x_b(n)$ . Thus, a medical specialist can visually verify the timing in each respiration phase. The expiration mask  $mexp_b(n)$  is:

$$mexp_b(n) = \begin{cases} 0.7 & , \quad p1_b(i) \leq n \leq p2_b(i), \forall i \\ -0.2 & , \quad otherwise \end{cases}$$

for  $n = 0, 1, \dots, NSB - 1$  (30)

The inspiration mask  $minsp_b(n)$  is

$$minsp_b(n) = \begin{cases} 0.35 & , \quad p3_b(i) \leq n \leq p4_b(i) \forall i \\ -0.2 & , \quad otherwise \end{cases}$$
(31)

The values 0.7, 0.35 and -0.2 were chosen to adequately visualize  $mexp_b(n)$  and  $minsp_b(n)$  when plotted next to  $x_b(n)$ . Figure 11 shows the graph of  $x_b(n)$  in blue,  $mexp_b(n)$  in red and  $minsp_b(n)$  in green. These masks can be used to segment the waveform for each respiration phase in each period. Thus, future works can use this segmentation for feature extraction and pathology detection via respiratory nasal or buccal acoustic signals.

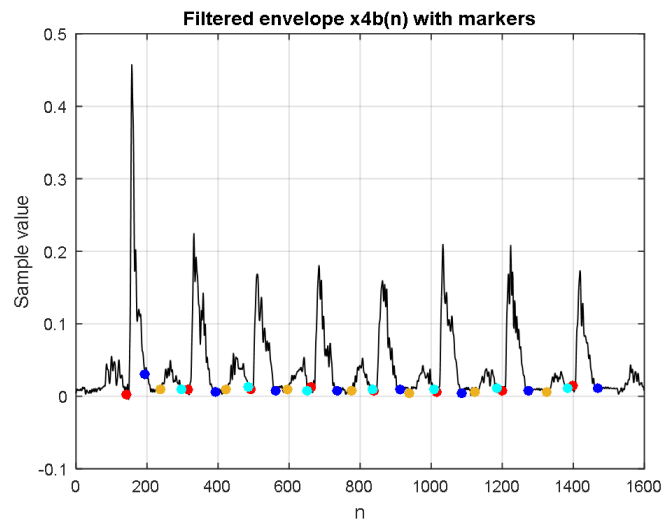


Figure 10. Filtered envelope  $x4_b(n)$  with markers at each expiration interval: red (start) and blue (end), with markers at each inspiration interval: yellow (start) and light blue (end)

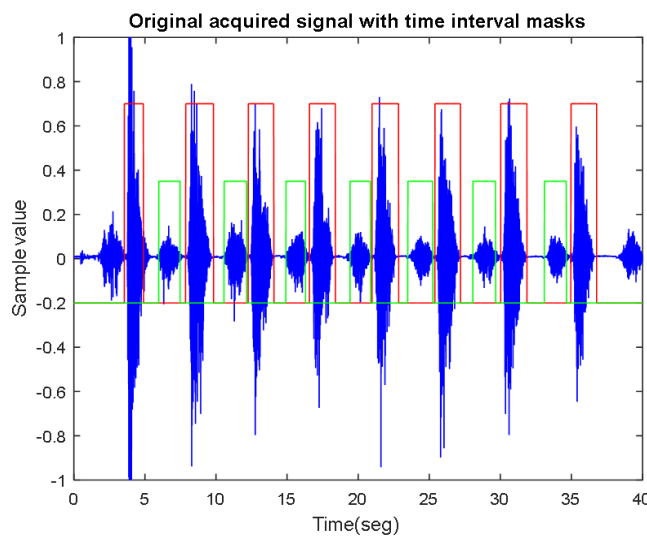


Figure 11. Original acquired signal (blue) with expiration (red) and inspiration (green) time interval masks

### 3. RESULTS AND DISCUSSION

Three signal acquisition masks were built for algorithm validation purposes. Three people using each their own mask generated the signal samples. A multimedia card and a personal computer were employed to acquire the signals. Person 1 generated 13 signals, Person 2 generated 12 signals and Person 3 generated 7 signals. Each person was adequately instructed regarding the following procedure:

Step 1: The person puts the mask on.

Step 2: A verification of correct mask placement is performed.

Step 3: The mask is connected to the audio card in the personal computer.

Step 4: Three seconds of a “silence” signal is captured by asking the person to not breathe. This serves a “floor” noise level.

Step 5: The person is indicated that the acquisition is starting, and they are asked to breath at a low, medium, or high frequency. This was accorded previously with each person.

Step 6: The signal acquisition process is performed for 80 seconds, to obtain two 40 second blocks with enough periods to get well defined frequency components.

After building the dataset, each signal was visually inspected and the breathing period, inspiration and expiration timings and the breathing rate were manually labeled in the signal. The beginning and ending of each time interval employed the floor noise level estimated in step 4 of the acquisition procedure. *BR*, *BP*, *AIT* and *AET*, the average time and frequency values of the algorithm, were manually determined for each signal. Performing the validation with a spirometer was not feasible and thus this option was discarded. It required the simultaneous acquisition of the sound and the air flow emitted by the person, which was quite difficult. The relative error percentage was used to compare the algorithm results with the manual measurements [29],

$$\%Error = \left| \frac{Vpa - Vm}{Vm} \right| \times 100 \quad (32)$$

where *Vpa* is the value estimated by the proposed algorithm and *Vm* is the value obtained via the manual method. Tables 1, 2, and 3 show the results for each person. Figures 12, 13, and 14 show the relative error graphs for each person and signal.

Table 1. Measurement results for Person 1

Signal	Manual				Proposed Algorithm				Error (%)			
	<i>BR</i> (cycles/min)	<i>BP</i> (seg)	<i>AIT</i> (seg)	<i>AET</i> (seg)	<i>BR</i> (cycles/min)	<i>BP</i> (seg)	<i>AIT</i> (seg)	<i>AET</i> (seg)	<i>BR</i>	<i>BP</i>	<i>AIT</i>	<i>AET</i>
1	14.33	4.19	1.57	1.78	14.06	4.27	1.52	1.82	1.88	1.91	3.22	2.14
2	11.23	5.34	1.47	1.56	11.72	5.12	1.40	1.50	4.34	4.16	4.88	4.36
3	14.01	4.28	1.54	1.62	14.06	4.27	1.51	1.66	0.35	0.34	1.69	2.47
4	14.03	4.27	1.68	1.64	14.06	4.27	1.70	1.65	0.23	0.23	0.87	0.71
5	13.81	4.34	1.64	1.64	14.06	4.27	1.68	1.67	1.78	1.75	2.10	2.11
6	12.19	4.92	1.36	1.55	11.72	5.12	1.37	1.63	3.92	4.08	0.44	4.82
7	11.70	5.13	1.72	1.84	11.72	5.12	1.78	1.81	0.12	0.12	3.16	1.74
8	13.33	4.50	1.68	1.59	13.28	4.52	1.70	1.66	0.39	0.39	1.00	4.82
9	12.04	4.98	1.69	1.76	11.72	5.12	1.64	1.81	2.67	2.74	2.81	2.89
10	8.93	6.72	1.71	1.89	8.59	6.98	1.64	2.00	3.75	3.90	4.10	5.89
11	9.78	6.14	1.77	1.89	9.38	6.40	1.87	1.95	4.14	4.32	5.59	3.44
12	9.19	6.53	1.76	2.12	9.38	6.40	1.79	2.12	2.00	1.97	1.82	0.34
13	9.82	6.11	1.82	1.79	10.16	5.91	1.84	1.78	3.47	3.35	1.31	0.83

Table 2. Measurement results for Person 2

Signal	Manual				Proposed Algorithm				Error (%)			
	<i>BR</i> (cycles/min)	<i>BP</i> (seg)	<i>AIT</i> (seg)	<i>AET</i> (seg)	<i>BR</i> (cycles/min)	<i>BP</i> (seg)	<i>AIT</i> (seg)	<i>AET</i> (seg)	<i>BR</i>	<i>BP</i>	<i>AIT</i>	<i>AET</i>
1	19.66	3.05	1.11	1.30	18.75	3.20	1.04	1.36	4.62	4.84	6.56	4.46
2	19.46	3.08	0.98	1.19	18.75	3.20	0.94	1.24	3.64	3.78	4.07	4.18
3	19.05	3.15	1.22	1.42	18.75	3.20	1.25	1.45	1.56	1.58	2.84	2.03
4	16.67	3.60	1.11	1.65	16.41	3.66	1.10	1.67	1.58	1.60	0.80	1.43
5	16.66	3.60	1.11	1.35	16.41	3.66	1.13	1.33	1.52	1.55	1.63	1.50
6	19.43	3.09	1.08	1.49	18.75	3.20	1.03	1.54	3.52	3.65	5.28	3.52
7	18.87	3.18	1.13	1.39	18.75	3.20	1.12	1.41	0.61	0.62	0.85	1.31
8	16.43	3.65	1.47	1.77	16.41	3.66	1.49	1.76	0.16	0.16	1.56	0.84
9	11.75	5.11	1.84	1.88	11.72	5.12	1.85	1.89	0.25	0.25	0.42	0.78
10	16.61	3.61	1.31	1.62	16.41	3.66	1.38	1.70	1.24	1.26	6.04	4.91
11	18.86	3.18	1.00	1.32	18.75	3.20	1.07	1.36	0.56	0.57	6.73	3.30
12	21.40	2.80	0.70	1.20	21.09	2.84	0.74	1.24	1.43	1.45	4.89	3.33

Table 3. Measurement results for Person 3

Signal	Manual				Proposed Algorithm				Error (%)			
	<i>BR</i> (cycles/min)	<i>BP</i> (seg)	<i>AIT</i> (seg)	<i>AET</i> (seg)	<i>BR</i> (cycles/min)	<i>BP</i> (seg)	<i>AIT</i> (seg)	<i>AET</i> (seg)	<i>BR</i>	<i>BP</i>	<i>AIT</i>	<i>AET</i>
1	18.51	3.24	0.63	0.95	18.75	3.20	0.66	0.98	1.31	1.29	4.74	2.60
2	11.98	5.01	1.32	1.51	11.72	5.12	1.36	1.53	2.19	2.23	3.06	1.66
3	14.02	4.28	1.40	1.40	14.06	4.27	1.38	1.42	0.31	0.31	1.28	0.88
4	7.22	8.31	2.59	2.90	7.03	8.53	2.68	2.98	2.60	2.67	3.65	2.76
5	11.98	5.01	1.71	1.57	11.72	5.12	1.76	1.60	2.20	2.25	3.06	2.25
6	14.27	4.21	1.31	1.38	14.06	4.27	1.39	1.41	1.43	1.45	6.29	2.47
7	11.66	5.15	1.80	1.70	11.72	5.12	1.77	1.68	0.53	0.53	1.87	1.55

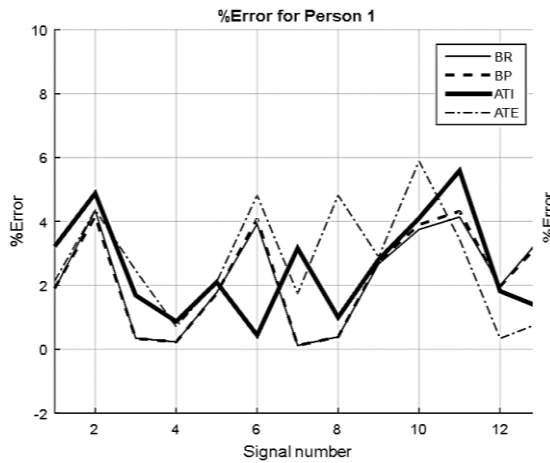


Figure 12. % Error for Person 1

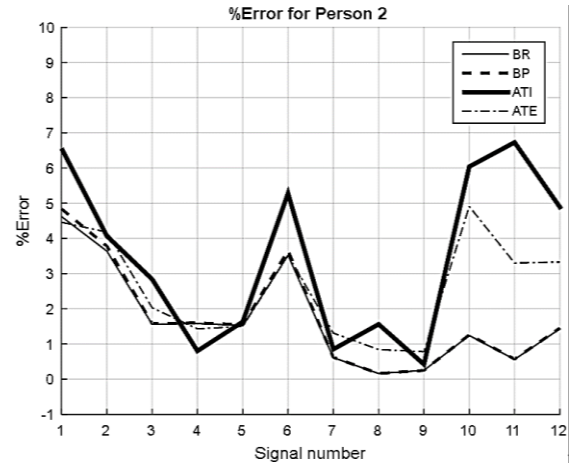


Figure 13. % Error for Person 2

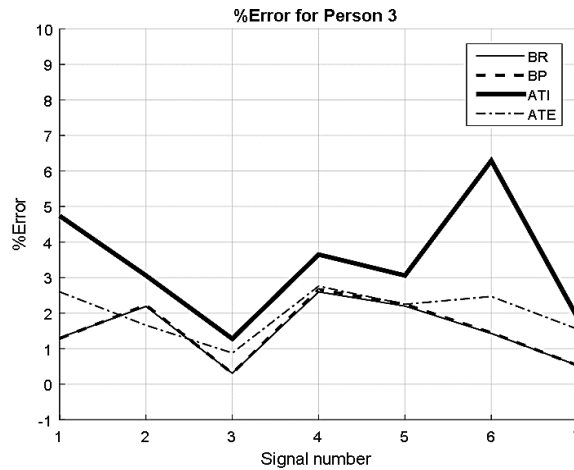


Figure 14. % Error for Person 3

The following statements can be derived from the results: i) the relative error for times and frequencies spans a range from 0% to 7%. This is highly satisfactory since it translates to a minimum precision of 93%; ii) using two microphones for the acquisition method positively impacted the quality of the obtained results; iii) verifiably, the relative error is independent from the breathing rate of each person and from the inspiration and expiration time intervals; iv) in most cases, the inspiration times present the highest errors (although less than 7%). This can be explained because inspiration times are shorter than expiration times and much more susceptible to noise and distortion; v) the microphone acquisition circuit did not use any passive elements to minimize noise or distortion effects and the mask cost. Nonetheless, this circuit could be modified to evaluate if this can reduce the range of the relative error; and vi) finally, Table 4 shows the average relative error percentages for each person. For *BR*, the maximum average relative error percentage is

2.23% (Person 1); for *BP*, it is 2.25% (Person 1); for *AIT*, it is 3.47% (Person 2); and for *AET*, it is 2.81% (Person 1).

Table 4. Average % Error

Person	Average % Error <i>BR</i>	Average % Error <i>BP</i>	Average % Error <i>AIT</i>	Average % Error <i>AET</i>
Person 1	<b>2.23</b>	2.25	2.54	<b>2.81</b>
Person 2	1.72	1.77	<b>3.47</b>	2.63
Person 3	1.51	1.53	3.42	2.02

#### 4. CONCLUSION

The proposed algorithm was developed in Python and implemented in both a web server and a small single-board computer. Regarding the server implementation, the signal was acquired through an Android smartphone connected to the acquisition mask via a purpose-built application. In it, the person registers as a patient, configures the acquisition time and starts the acquisition in a low-noise, relaxed place. The signal is stored in a waveform audio (WAV) file. Then, it is uploaded to the server with the date, time, and personal data of the patient. The server processes the signal and registers the results. These results can be viewed in both a desktop and mobile application. A medical professional can then visualize these results and add notes with the diagnostic and commentaries. In this implementation, the system can be employed for remotely monitoring patients with respiratory ailments and aid in their correct control without the need of commuting to the health establishment.

Regarding the single-board computer implementation, it serves as a first step to develop portable respiratory evaluation equipment that patients can use in health establishments. The successful results motivated the development of the stated applications. Finally, the time masks which the algorithm outputs can be used by future projects which aim to identify respiratory pathologies or perform estimations of the volume of inspired air and expired air as determined by a spirometer. Thus, the developed applications can have new functionalities to aid medical professionals in reducing their time to diagnosis.

#### ACKNOWLEDGEMENTS

The authors would like to thank the Research Department of the Peruvian University of Applied Science for technical and economic support.




#### REFERENCES

- [1] M. A. Islam, I. Bandyopadhyaya, P. Bhattacharyya, and G. Saha, "Multichannel lung sound analysis for asthma detection," *Computer Methods and Programs in Biomedicine*, vol. 159, pp. 111–123, Jun. 2018, doi: 10.1016/j.cmpb.2018.03.002.
- [2] A. Sovijarvi, "Characteristics of breath sounds and adventitious respiratory sounds," *Eur Respir Rev*, pp. 591–596, 2000.
- [3] H. Pasterkamp, S. S. Kraman, and G. R. Wodicka, "Respiratory sounds," *American Journal of Respiratory and Critical Care Medicine*, vol. 156, no. 3, pp. 974–987, Sep. 1997, doi: 10.1164/ajrccm.156.3.9701115.
- [4] Z. Neili, M. Fezari, and A. Redjati, "ELM and K-NN machine learning in classification of breath sounds signals," *International Journal of Electrical and Computer Engineering (IJECE)*, vol. 10, no. 4, pp. 3528–3536, Aug. 2020, doi: 10.11591/ijece.v10i4.pp3528-3536.
- [5] M. E. Wechsler, "Managing asthma in primary care: putting new guideline recommendations into context," *Mayo Clinic Proceedings*, vol. 84, no. 8, pp. 707–717, Aug. 2009, doi: 10.4065/84.8.707.
- [6] Y. Nam, B. A. Reyes, and K. H. Chon, "Estimation of respiratory rates using the built-in microphone of a smartphone or headset," *IEEE Journal of Biomedical and Health Informatics*, vol. 20, no. 6, pp. 1493–1501, Nov. 2016, doi: 10.1109/JBHI.2015.2480838.
- [7] S.-H. Li, B.-S. Lin, C.-H. Tsai, C.-T. Yang, and B.-S. Lin, "Design of wearable breathing sound monitoring system for real-time wheeze detection," *Sensors*, vol. 17, no. 12, Jan. 2017, doi: 10.3390/s17010171.
- [8] O. Yahya and M. Faezipour, "Automatic detection and classification of acoustic breathing cycles," in *Proceeding 2014 Zone 1 Conference of the American Society for Engineering Education*, Bridgeport, CT, USA, 3–5 April 2014, doi: 10.1109/aseezone1.2014.6820648.
- [9] Y. Nam, J. Lee, and K. H. Chon, "Respiratory rate estimation from the built-in cameras of smartphones and tablets," *Annals of Biomedical Engineering*, vol. 42, no. 4, pp. 885–898, Apr. 2014, doi: 10.1007/s10439-013-0944-x.
- [10] S. Chatterjee, M. M. Rahman, E. Nemanti, and J. Kuang, "WheezeD: respiration phase-based wheeze detection using acoustic data from pulmonary patients under attack," in *Proceeding 13th EAI International Conference on Pervasive Computing Technologies for Healthcare-Demos and Posters*, European Alliance for Innovation (EAI), 2019, doi: 10.4108/eai.20-5-2019.2283516.
- [11] D. S. Avalur, "Human breath detection using a microphone," M.S. thesis, Faculty of Mathematics and Natural Sciences, University of Groningen, 2013.
- [12] O. I. R. Diaz *et al.*, "Mobile application for temporal, spectral and time-frequency analysis of continuous adventitious breath sounds (in Spanish)," in *Memorias del Congreso Nacional de Ingeniería Biomédica*, vol. 5, no. 1, pp. 78–81, 2018.
- [13] C. Daluwatte, C. G. Scully, G. C. Kramer, and D. G. Strauss, "A robust detection algorithm to identify breathing peaks in respiration signals from spontaneously breathing subjects," in *2015 Computing in Cardiology Conference (CinC)*, Sep. 2015,




- pp. 297–300, doi: 10.1109/CIC.2015.7408645.
- [14] F. Javed, H. Fox, and J. Armitstead, “ResCSRf: algorithm to automatically extract Cheyne-stokes respiration features from respiratory signals,” *IEEE Transactions on Biomedical Engineering*, vol. 65, no. 3, pp. 669–677, Mar. 2018, doi: 10.1109/TBME.2017.2712102.
  - [15] S. M. M. Islam and V. M. Lubecke, “Extracting individual respiratory signatures from combined multi-subject mixtures with varied breathing pattern using independent component analysis with the JADE algorithm,” in *2020 IEEE Asia-Pacific Microwave Conference (APMC)*, Dec. 2020, pp. 734–736, doi: 10.1109/APMC47863.2020.9331715.
  - [16] W. Sun, M. Jiang, G. Chen, and T. You, “A comparison of adaptive boosting algorithms for the respiratory signal prediction,” in *2019 12th International Congress on Image and Signal Processing, BioMedical Engineering and Informatics (CISP-BMEI)*, Oct. 2019, pp. 1–5, doi: 10.1109/CISP-BMEI48845.2019.8965954.
  - [17] F. Guede-Fernandez, M. Fernandez-Chimeno, J. Ramos-Castro, and M. A. Garcia-Gonzalez, “Driver drowsiness detection based on respiratory signal analysis,” *IEEE Access*, vol. 7, pp. 81826–81838, 2019, doi: 10.1109/ACCESS.2019.2924481.
  - [18] Y. Zhivolupova, “Sleep apnea and hypopnea detection algorithm,” in *2019 Ural Symposium on Biomedical Engineering, Radioelectronics and Information Technology (USBREIT)*, Apr. 2019, pp. 90–93, doi: 10.1109/USBREIT.2019.8736554.
  - [19] E. Saatci and E. Saatci, “Determination of respiratory parameters by means of hurst exponents of the respiratory sounds and stochastic processing methods,” *IEEE Transactions on Biomedical Engineering*, vol. 68, no. 12, pp. 3582–3592, Dec. 2021, doi: 10.1109/TBME.2021.3079160.
  - [20] D. Oletic and V. Bilas, “Asthmatic wheeze detection from compressively sensed respiratory sound spectra,” *IEEE Journal of Biomedical and Health Informatics*, vol. 22, no. 5, pp. 1406–1414, Sep. 2018, doi: 10.1109/JBHI.2017.2781135.
  - [21] E.-A. Paraschiv and C.-M. Rotaru, “Machine learning approaches based on wearable devices for respiratory diseases diagnosis,” in *2020 International Conference on e-Health and Bioengineering (EHB)*, Oct. 2020, pp. 1–4, doi: 10.1109/EHB50910.2020.9280098.
  - [22] Y. Wang *et al.*, “Low-cost and unobtrusive respiratory condition monitoring based on Raspberry Pi and recurrent neural network,” in *2021 IEEE International Symposium on Circuits and Systems (ISCAS)*, May 2021, pp. 1–5, doi: 10.1109/ISCAS51556.2021.9401084.
  - [23] P. Bokov, B. Mahut, P. Flaud, and C. Delclaux, “Wheezing recognition algorithm using recordings of respiratory sounds at the mouth in a pediatric population,” *Computers in Biology and Medicine*, vol. 70, pp. 40–50, Mar. 2016, doi: 10.1016/j.compbiomed.2016.01.002.
  - [24] G. Sierra, V. Telfort, B. Popov, L. G. Durand, R. Agarwal, and V. Lanzo, “Monitoring respiratory rate based on tracheal sounds. First experiences,” in *The 26th Annual International Conference of the IEEE Engineering in Medicine and Biology Society*, vol. 3, pp. 317–320, doi: 10.1109/IEMBS.2004.1403156.
  - [25] A. Herbert, J. Pearn, and S. Wilson, “Normal percentiles for respiratory rate in children-reference ranges determined from an optical sensor,” *Children*, vol. 7, no. 10, Oct. 2020, doi: 10.3390/children7100160.
  - [26] A. Rizal, R. Hidayat, and H. A. Nugroho, “Signal domain in respiratory sound analysis: methods, application and future development,” *Journal of Computer Science*, vol. 11, no. 10, pp. 1005–1016, Oct. 2015, doi: 10.3844/jcssp.2015.1005.1016.
  - [27] G. Kemper, D. Ponce, J. Telles, and C. del Carpio, “An algorithm to obtain boat engine RPM from passive sonar signals based on DEMON processing and wavelets packets transform,” *Journal of Electrical Engineering and Technology*, vol. 14, no. 6, pp. 2505–2521, Nov. 2019, doi: 10.1007/s42835-019-00260-4.
  - [28] A. V Oppenheim, J. R. Buck, and R. W. Schaffer, *Discrete-time signal processing*. Upper Saddle River, NJ: Prentice Hall, 2001.
  - [29] S. Kim and H. Kim, “A new metric of absolute percentage error for intermittent demand forecasts,” *International Journal of Forecasting*, vol. 32, no. 3, pp. 669–679, Jul. 2016, doi: 10.1016/j.ijforecast.2015.12.003.

## BIOGRAPHIES OF AUTHORS






**Guillermo Kemper**    received the B.S. degree in Electrical Engineering in 1994 from the Antenor Orrego Private University (UPAO), Trujillo, Peru. In years 1996 and 2001 he obtained a Master and a Ph.D. degree in Electrical and Communications Engineering respectively. Both degrees from the State University of Campinas (UNICAMP), Brazil. He has taken part for more than 3 years in the research agreement between the CPqD-Telebras (Brazilian Telecommunications Company) and UNICAMP, developing and designing audio and video coders. Currently, he is working as a research professor at the Electrical Engineering Program of the Peruvian University of Applied Sciences (UPC) in Lima, Peru. In addition, he is a researcher at the National Institute of Research and Training in Telecommunications (INICTEL). His research interests include voice, audio, images, and video processing, as well as digital communications and digital television. He can be contacted at email: guillermo.kemper@upc.pe.






**Angel Oshita**    received the in 2020 bachelor’s degree in electronic engineering from the Peruvian University of Applied Sciences, Lima, Perú. Since 2021, I have worked at telecommunication company called Infratel in the IT area, performing the role of web developer and data management. He can be contacted at email: u201511153@upc.edu.pe.



**Ricardo Parra**    received the in 2020 bachelor's degree in electronic engineering from the Peruvian University of Applied Sciences, Lima, Perú. Since 2019, I have worked at Banco de Credito del Peru in the IT area, performing the role of access and operations administrator. Also, this year, I participated in a project for a telephone company as a data warehouse analyst and as a data engineer in a mining machinery supplier company called Komatsu Mitsui. He can be contacted at email: u201411690@upc.edu.pe.



**Carlos Herrera**    received a bachelor's degree in Electronic Engineering in 2016 from Universidad San Martín de Porres (USMP), Lima, Peru. He provided services in hardware design for the development of the SMATCEL device at the National Institute for Research and Training in Telecommunications (INICTEL). In addition, he completed certified studies in Machine Learning with Python at the National Institute for Research and Training in Telecommunications (INICTEL) in 2020. He was a research assistant member of the Phukuy Project, a Digital Spirometer developed by the Research Directorate of the Peruvian University of Applied Sciences (UPC) in years 2020-2021. Also, this year, he studies the Embedded Systems Specialization as part of the master's degree in the Faculty of Engineering of the University of Buenos Aires (FIUBA). His research interests include embedded systems development, signal processing, digital image processing and artificial intelligence applications. He can be contacted at email: carlos.herrera.trujillo@gmail.com.